quantum beam science

MDPI

Article

In Situ Analysis of the Phase Transformation Kinetics in the β-Water-Quenched Ti-5Al-5Mo-5V-3Cr-1Zr Alloy during Ageing after Fast Heating

Rafael Paiotti Marcondes Guimarães [1,2], Bruna Callegari [1], Fernando Warchomicka [2], Katherine Aristizabal [3], Flavio Soldera [3], Frank Mücklich [3] and Haroldo Cavalcanti Pinto [1,*]

1 Department of Materials Engineering, São Carlos School of Engineering, University of São Paulo, Av. João Dagnone, 1100, 13563-120 São Carlos, SP, Brazil; rafael.paiotti@tugraz.at (R.P.M.G.); bruna2.callegari@usp.br (B.C.)

2 Institute of Materials Science, Joining and Forming, Graz University of Technology, Kopernikusgasse 24, 8010 Graz, Austria; fernando.warchomicka@tugraz.at

3 Department of Materials Science and Engineering, Saarland University, Campus D3.3, 66123 Saarbrücken, Germany; katherine.aristizabal@uni-saarland.de (K.A.); f.soldera@matsci.uni-saarland.de (F.S.); muecke@matsci.uni-sb.de (F.M.)

* Correspondence: haroldo@sc.usp.br

Received: 31 October 2019; Accepted: 11 February 2020; Published: 21 February 2020

Abstract: Thermal treatments are the main route to achieve improvements in mechanical properties of β-metastable titanium alloys developed for structural applications in automotive and aerospace industries. Therefore, it is of vital importance to determine phase transformation kinetics and mechanisms of nucleation and precipitation during heat treatment of these alloys. In this context, the present paper focuses on the assessment of solid-state transformations in a β-water-quenched Ti-5Al-5Mo-5V-3Cr-1Zr alloy during the early stages of ageing treatment at 500 °C. In situ tracking of transformations was performed using high-energy synchrotron X-ray diffraction. The transformation sequence $\beta + \omega \rightarrow \alpha + \alpha''_{iso} + \beta$ is proposed to take place during this stage. Results show that isothermal α″ phase precipitates from ω and from spinodal decomposition domains of the β phase, whereas α nucleates from ω, β and also from α″ with different morphologies. Isothermal α″ is considered to be the regulator of transformation kinetics. Hardness measurements confirm the presence of ω, although this phase was not detected by X-ray diffraction during the in situ treatment.

Keywords: high-energy X-ray diffraction; near-beta titanium alloys; ageing; Rietveld refinement; spinodal decomposition; metastable phases; Ti-55531

1. Introduction

The search for structural materials and products with advanced technology and quality has increasingly taken into consideration characteristics such as strength-to-weight ratio, corrosion resistance, machining cost, and absence of toxic elements. Several materials comply with these requirements in service, including many titanium-based alloys. In medical (e.g., in orthopedic implants) and in aerospace applications, beta (β) titanium alloys are intensively used due to their low elastic modulus, good formability, high fatigue strength, and resistance to crack propagation [1].

The near-beta alloy Ti-10V-2Fe-3Al (Ti-10-2-3) is the leading structural material in terms of mechanical strength. However, its application is limited by its complex processing requirements, with a considerable number of variables, and by its sensitivity to slight composition and temperature variations [1]. In this context, the metastable β alloy Ti-5Al-5Mo-5V-3Cr-1Zr (Ti-55531) was developed based on the pioneering VT-22 (Ti-6Al-5V-5Mo-1Cr-1Fe) Russian alloy [2]. Its relevance relies on its

wide thermomechanical processing window, through which considerable improvements in mechanical properties can be achieved [3–5]. In comparison with Ti-10-2-3, the alloy is less sensitive to thermal variations and to deformation rates [3].

Microstructural evolution of Ti-55531 alloy in the β-quenched condition during continuous heating under different rates was studied by Barriobero-Vila et al. [3]. Their work evidenced the influence of the heating rate on the phase transformation kinetics. During slow heating (5 °C/min), martensitic orthorhombic α″ phase precipitates from omega (ω) phase in the temperature range of 400–450 °C. When the heating rate increases, this precipitation is retarded. Subsequently, α″ phase transforms into α phase between 600 and 650 °C influenced by the diffusion of β-stabilizing elements from α″ to the β matrix; this explains the metastability of α during its early stages in the alloy. In the aforementioned work, the alloy exhibited direct precipitation of α from β phase above 650 °C when a heating rate of 100 °C/min was employed, since the fast heating rate inhibits the formation of metastable phases. Other studies of phase transformations in as-quenched β-metastable alloys during heating have shown that increasingly higher rates make the distribution of α″ and α phase more homogeneous within the β matrix [4,6–9], apart from minimizing precipitation. Ivasishin et al. have outlined that microstructural morphology, distribution, and resulting precipitation sequences during ageing treatments are intimately connected to the initial conditions of the alloy and to the heating rate up to the treatment temperature [6]. They established that β alloys with fine-grained initial condition have a faster aging response due to residual defects and/or stresses, since this leads to the acceleration of the nucleation of precipitates and the diffusion of alloying elements. In addition, the role of ω in the precipitation of α phase was clarified, leading to the conclusion that inducing ω precipitation by means of slow heating or intermediate ageing steps at lower temperatures is desirable to provide the precipitation of fine α, thus enhancing mechanical properties.

Although important studies focused on the solid-state phase transformation sequences in β titanium alloys have already been conducted, knowledge of the real basis of governing mechanisms responsible for formation and decomposition of both stable and metastable phases is still considerably limited. Most works on microstructural evolution make use of conventional techniques such as dilatometry, differential scanning calorimetry, electrical resistivity, and X-ray diffraction to characterize phase transformation kinetics [10–12]. Analyses using these techniques are not always complete or easily carried out and interpreted. However, the development of high-energy X-ray diffraction (HEXRD) using synchrotron radiation allows real-time (in situ) observation of microstructural evolution and phase transformations [3,6,10,11,13,14]. HEXRD presents the advantage of short acquisition times and high resolution, and for this reason has gained momentum in the metallurgy area for providing the possibility of precisely elucidating phase transformation phenomena [11,12,15].

The present paper aims to investigate the kinetics and mechanisms of precipitation and decomposition of stable and metastable phases in a Ti-5Al-5Mo-5V-3Cr-1Zr alloy with a starting β-quenched microstructure during ageing using in situ high-energy X-ray diffraction as the main tool to keep track of such transformations. A typical ageing temperature of 500 °C was chosen for the investigation, which focuses on the early stages of transformations during heat treatment, when the formation and decomposition of metastable phases mainly takes place.

2. Materials and Methods

The investigated material was a β-metastable alloy, Ti-5Al-5Mo-5V-3Cr-1Zr (Ti-55531), with the following chemical composition in wt%: 5.51Al, 5.01Mo, 5.04V, 2.85Cr, 1.125Zr, 0.32Fe, 0.0665O, 0.0085N, 0.0045C and balance Ti. The $[Mo]_{eq}$ for this alloy is 8.36 [16] and the β-transus temperature of the alloy is 803 °C, as reported in [3]. Solution treatment in the β field was carried out at 900 °C for 20 min in dynamic argon atmosphere followed by quenching in water at room temperature. This β-quenched condition represents the initial condition for heating and subsequent aging.

In situ high-energy X-ray diffraction was carried out at the ID15B beamline of the European Synchrotron Radiation Facility (ESRF), in Grenoble, France. The experiments were performed in

transmission mode with energy E = 87 keV (λ = 0.0142 nm) and a slit aperture size of 300 × 300 μm^2. The diffraction images were collected in a in a Pixium® Image Plate detector, with an acquisition time set to 5 s and a readout time of 1 s. The sample-detector distance was set to 1252 mm and the instrumental broadening was calibrated with a LaB_6 capillary placed at the same distance. Samples with dimensions of 4 × 4 × 20 mm^3 were cut from the quenched alloy and heat treated in the beamline by means of a radiant furnace with argon atmosphere. The isothermal heat treatment was carried out at 500 °C for 3600 s, after heating at 300 °C/min from room temperature (RT). The selected temperature of analysis is based on the processing of components made from metastable β titanium alloys (e.g., Ti-17, Ti-10V-2Fe-3Al, Ti-5553 family) [1] and on previous works with fast cooling from the beta region [4,17]. In general, the window of ageing treatment temperatures is between 500 and 600 °C to prevent the presence of isothermal ω (hard and brittle phase) in the final condition. In this work, the lowest commercial temperature was used to analyze the first 3600 s of ageing treatment after fast heating from a β-metastable condition. The use of a fast heating rate aims to avoid the formation of the isothermal ω phase during heating.

Sequences of complete Debye–Scherrer rings from the bulk of the sample were acquired in transmission mode using a 2D image plate detector, and the temperature was controlled by a spot-welded thermocouple located close to the probed spot in the sample. Instrumental calibration was carried out using a LaB_6 powder standard. Data were processed using FIT2D software [18]. Image sequences of Debye–Scherrer rings were analyzed qualitatively using ImageJ software [19]. Resulting diffraction patterns were refined via Rietveld's method using Materials Analysis Using Diffraction (MAUD) software [20] for extraction of quantitative information about phase transformations, such as lattice parameters and phase fractions. Table 1 presents crystallographic data of the phases considered in this paper for Rietveld refinement.

Table 1. Crystallographic data of phases considered for Rietveld refinement.

Phase	A (Å)	B (Å)	C (Å)	Structure	Space Group	Atomic Positions (x, y, z)	Reference
α	2.93	-	4.60	Hexagonal	$P6_3/mmc$	(1/3, 2/3, 1/4) (2/3, 1/3, 3/4)	[21]
β	3.23	-	-	Cubic	$Im\bar{3}m$	(0,0,0) (1/2, 1/2, 1/2)	[21]
ω	4.55	-	2.78	Hexagonal	P6/mmm	(0,0,0) (1/3, 2/3, 1/3 + z_ω) (2/3, 1/3, 2/3-z_ω); z_ω = 1/6	[22]
α″	3.00	4.97	4.56	Orthorhombic	Cmcm	(0, y, 1/4) (0, 1-y, 3/4) (1/2, $\frac{1}{2}$ + y, 1/4) (1/2, 1/2-y, 3/4); y_0 = 0.18	[23]

Treated samples were metallographically prepared for optical and scanning electron microscopies by grinding, polishing, and etching with Kroll's reagent (2% HF + 4% HNO_3 + 94% H_2O). Optical microscopy was carried out using a AxioScope microscope (Zeiss, Oberkochen, Germany) with an ERC 5s camera, and SEM was performed on a Inspect F50 microscope (FEI, Hillsboro, OR, USA) at 10 kV. TEM-thin lamellae of the β-water-quenched sample and of the sample aged at 500 °C during 1500 s were prepared by Focused Ion Beam (FIB) using a lift-out technique in a dual beam SEM/FIB Helios NanoLab 600 (FEI, Hillsboro, OR, USA). STEM and point quantitative chemical analyses by energy dispersive spectroscopy (EDS) were carried out in the lamellae using the same equipment. TEM analysis was performed in a TECNAI G2-F20 microscope (FEI, Hillsboro, OR, USA) with field emission gun operated at 200 kV.

Aged samples were subjected to Vickers micro-hardness testing in a PB1000 Mechanical Tester (Nanovea, Irvine, CA, USA). The load employed was 100 mN and the spacing between each indentation was 200 μm. In total, each sample was indented nine times.

3. Results

3.1. Initial Condition

Figure 1a reveals, by SEM, the microstructure of the β-water-quenched samples of the Ti-55531 alloy. One can notice equiaxed β-grains with a size in the range of 97 ± 55 μm. Figure 1b depicts a High-Angle Annular Dark-Field (HAADF) STEM image of the initial microstructure, in which bright and dark areas indicate the occurrence of spinodal decomposition (composition contrast). Table 2 presents the results of spot EDS analyses in each of these areas. It shows that the bright area is richer in β-stabilizing elements than the dark area. The evident variation in Mo content was also observed by Li et al. in a near-β alloy [24]. They have observed that ω formation kinetics is directly determined by coherent spinodal decomposition within the β phase, and that Mo compositional modulation directly influences the degree of plane collapse along <111> direction. During the displacive transformation, ω inherits the composition of β lean regions. Hence, metastable β-grains with the presence of spinodal decomposition and athermal ω (or ω_{ath}) phases compose the initial condition, as observed in the electron diffraction pattern of the [113] β zone (Figure 1c). For a deeper analysis of the initial condition, the reader is referred to the work of Barriobero-Vila et al. [3], since the material employed in both studies came from the same batch and same heat treatment procedure.

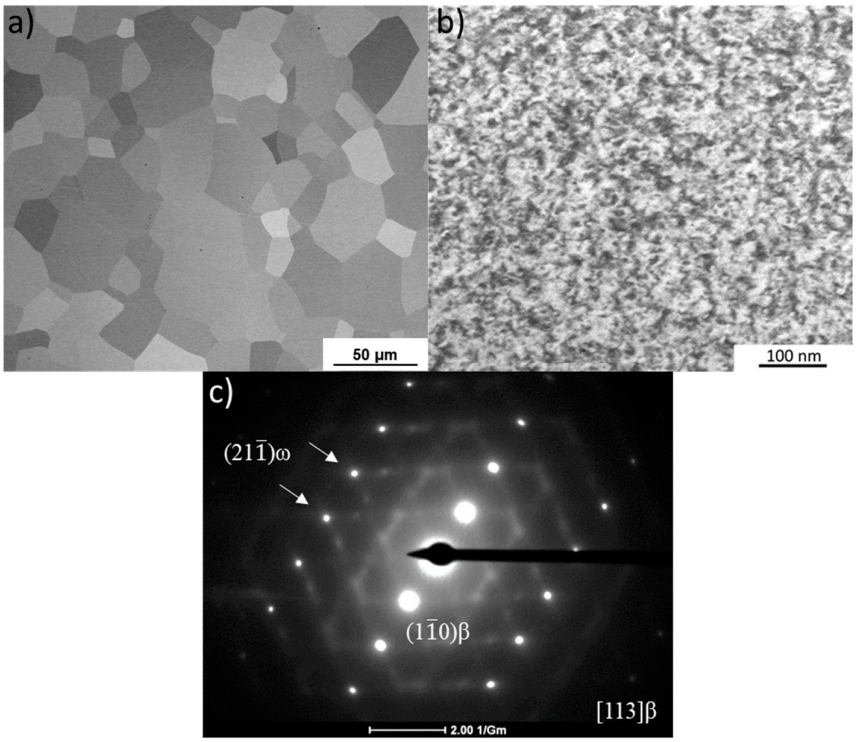

Figure 1. (**a**) Scanning electron microscopy image of the water-quenched microstructure and (**b**) High-Angle Annular Dark-Field (HAADF) STEM image of the initial microstructure showing evidence of spinodal decomposition, given by the contrast between bright and dark areas and (**c**) electron diffraction pattern of the (113)β zone axis showing spots of athermal ω.

Table 2. Results of EDS analyses in Figure 1 for the initial water-quenched condition of Ti-55531 alloy.

Area	**Composition (wt %)**					
	Ti	Al	Mo	V	Cr	Zr
Dark	82.6	5.2	4.3	4.5	2.4	1.0
Bright	79.9	5.5	5.6	5.0	2.9	1.1

3.2. In Situ Measurements

3.2.1. Influence of Heating Up to 500 °C

Figure 2 depicts two portions of the Debye–Scherrer rings converted to Cartesian coordinates corresponding to room temperature (RT) and 500 °C. One can notice the spots belonging to (110)β, (200)β, and (211)β reflections in both portions, as well as no visible changes on these during the heating step. In addition, no new reflections of phases such as α, α″, or ω were found. Thus, it can be stated that during the heating stage phase transformation might be hindered. It is in agreement with the findings of Barriobero-Villa, where a heating rate of 100 °C/min suppressed the transformation of the present alloy in the same starting condition up to 650 °C [3].

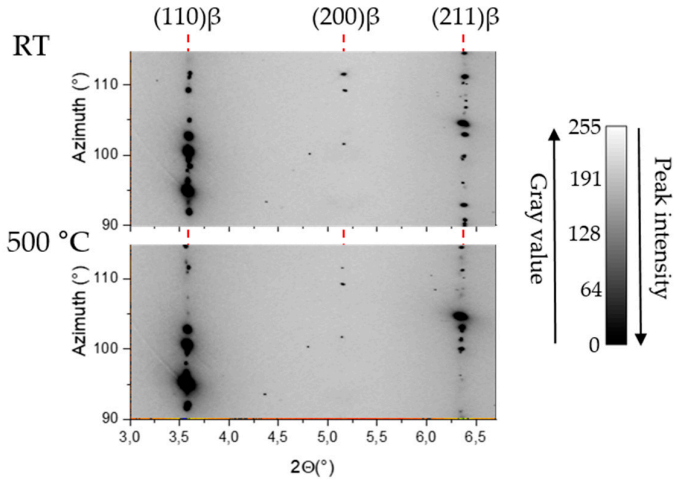

Figure 2. 2D plots of portions of Debye–Scherrer rings converted into Cartesian coordinates showing the behavior of spots corresponding to Bragg reflections for RT and 500 °C.

3.2.2. Phase Evolution during Ageing at 500 °C

Figure 3 presents representative quarters of Debye–Scherrer rings acquired during ageing at 500 °C in four moments: t = 0, 600, 1800, and 3600 s, clearly showing the phase evolution during treatment. At first glance one can notice the spotty aspect of rings at t = 0 s, indicating a coarse-grained initial microstructure that persists until t = 600 s. Between t = 600 s and t = 1800 s, these isolated spots align with each other as a consequence of microstructural evolution. At the same time, double rings start to appear close to (110)β corresponding to the precipitation of isothermal α″ (α''_{iso}) and α [4,6]. At t = 3600 s, the width of the rings increased as result of the rise in the amount of α''_{iso} and α. It is important to highlight that at t = 600 s one can observe weak reflections located close to {110}β (indicated by blue arrows), evidencing the precipitate–matrix orientation relationship [25].

Figure 4 presents a more clear and detailed evolution of {110}β spots and of the diffuse streaks. β spots experienced a decrease in intensity between t = 0 s and t = 140 s followed by an elongation from t = 196 s onwards. One may visualize different diffuse streaks in the Debye–Scherrer rings, where white arrows at t = 140 s point out the first signals of their appearance. At t = 265 and 377 s, the streaks are delimited by the U-shaped curves in order to improve the visualization; white dashed lines at t = 442 s indicate the direction of their growth. With regards to the reflections of α/α″, these become visible at t = 265 s and are shown in the red box. As reflections evolve (contoured by the U-shaped curves from t = 540 to 755 s), they assume aspects of double lines and they are indicated by the red double-dashed lines at t = 1192 s.

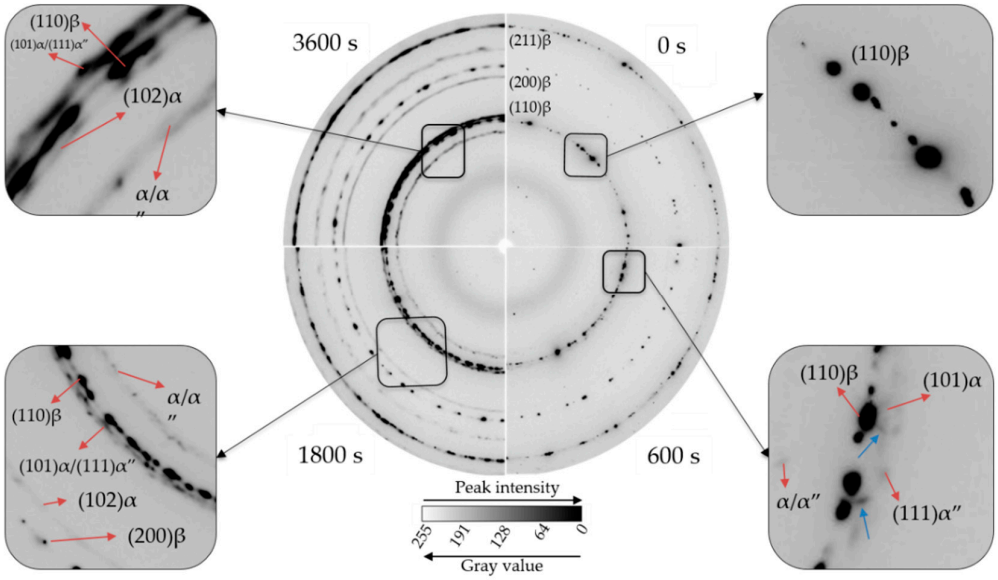

Figure 3. Representative quarters of Debye–Scherrer rings obtained during ageing for instants t = 0 s, t = 600 s, t = 1800 s, and t = 3600 s and respective phases observed, magnified 10 times in the respective boxes corresponding to each period of time. The diffuse inner ring observed corresponds to the scattering of a quartz capsule.

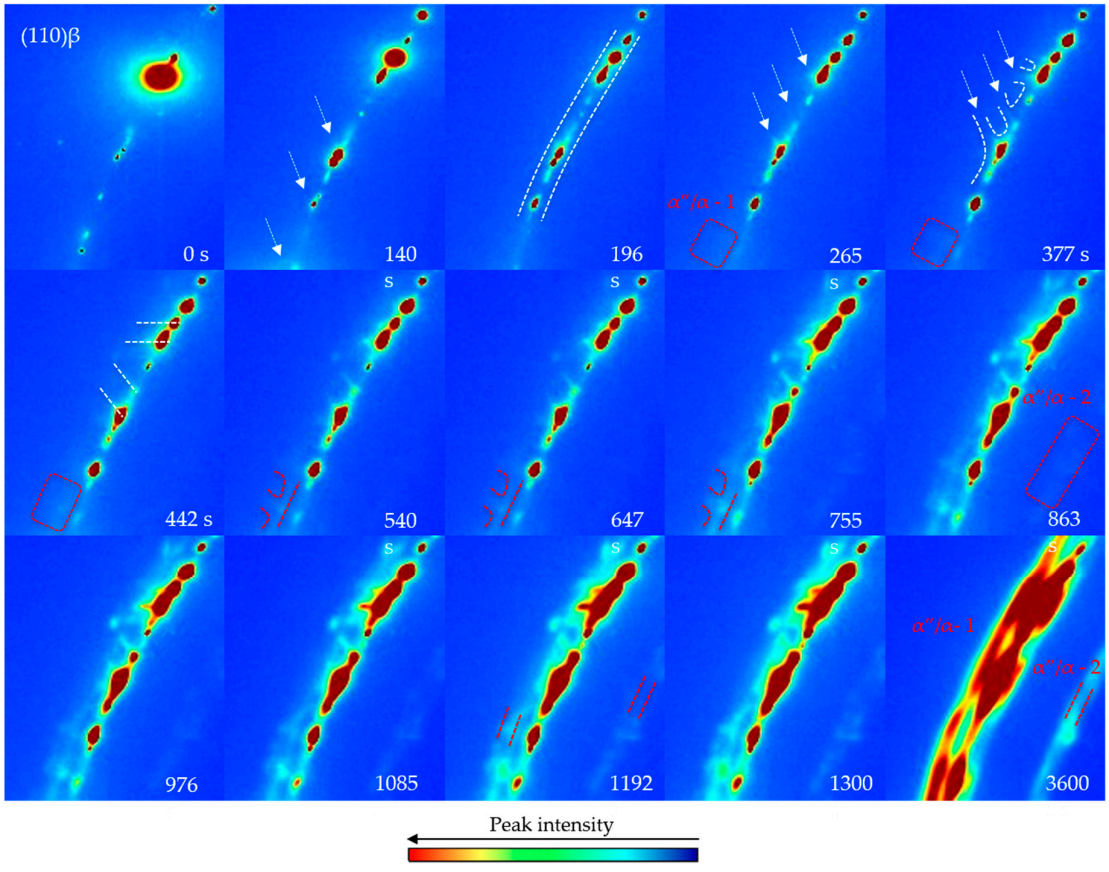

Figure 4. Sections extracted from the same areas of Debye–Scherrer rings depicting evolution of diffuse streaks (white arrows), their characteristic inclination (white dashed lines), and the appearance of double rings close to {110}β resulting from α and α''_{iso}.

Morphologically, the streaks from β → α/α″$_{iso}$ directions present themselves as thin, angularly similar, and continuous, expressing gradual and coherent evolution of lattice parameters of precipitating phases during ageing [25]. The distinction between α and α″$_{iso}$ spots in Figures 3 and 4 is difficult, since these phases precipitate within a considerably small 2θ interval (<0.5°). Furthermore, the chosen ageing temperature allows for precipitation of both phases, increasing the possibility of simultaneous precipitation onset or, at least, with too short a time difference for any distinction [3–5,26,27]. Therefore, it is plausible to propose that α and isothermal α″ have their first signs of reflection at t = 140 s, and that from this instant on diffusive β → α + α″$_{iso}$ transformation becomes active [4,25–28]. For this reason (and for refinement purposes), it is assumed that both phases begin to precipitate at the same instant. Lastly, at t = 3600 s, the dashed α/α″-2 red line in Figure 4 indicates duplicity, showing that the material may still contain α″$_{iso}$.

Figure 5 depicts 2D color-coded time vs. 2θ plots in the 2θ intervals 3.1–3.9°and 4.5–5.8° of the azimuthally integrated Debye–Scherrer rings aiming to improve the distinction between α and α″$_{iso}$. In both intervals, it is possible to observe reflections corresponding to α″$_{iso}$ from t = ~300 s and on. As mentioned before, these α″$_{iso}$ reflections (double peaks) also involve α reflections (single peak). Nonetheless, as the ageing progresses, these double peaks converge to single ones indicating the decomposition of α″$_{iso}$ to α [3,9,29,30]. In Figure 5a, at t = 2080 s (black arrow) the single {101}α peak becomes distinguishable from the set of reflections composed by {111}α″/{101}α/{021}α″.

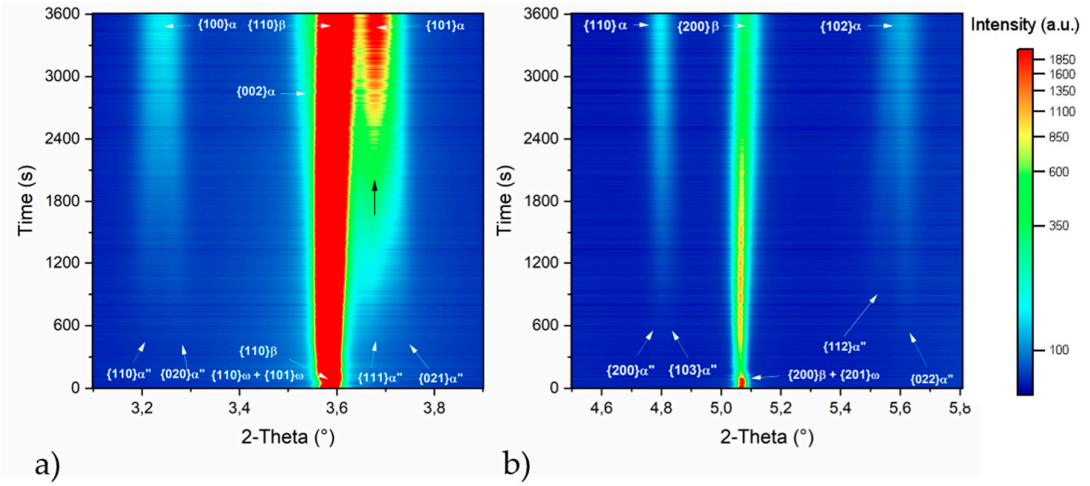

Figure 5. Color-coded plots showing the evolution of diffraction patterns as function of time during ageing for 2θ intervals between (**a**) 3.1 and 3.9° and (**b**) 4.5 and 5.8°. The evident appearance of {101}α reflection is indicated by the isolated black arrow.

One has to highlight that ω phase reflections were not directly observed in any of the images analyzed in this work. It could be due to (i) the superposition of the most intense ω peaks with more intense β peaks or (ii) to the weak and broad reflections resulting from its distorted crystal lattice [31,32] and/or to its low volume fraction. Likewise, ω phase is also located along dislocations formed between domains associated with β spinodal decomposition. The formation of such dislocations results in the distortion of β matrix lattice, hence its contribution is more significant to peak broadening, i.e., to the FWHM [33]. The difficulties for detection of ω phase are also reported for HEXRD studies [33,34]; nevertheless, recent observations carried out by high-energy small angle X-ray scattering during ageing in single crystals of metastable β titanium alloys could determine the presence and evolution of this phase [35–37].

3.2.3. Microhardness

Figure 6 shows the hardness evolution during ageing. Three distinct behaviors can be observed: (1) a slight increase up to t = 150 s, (2) a decrease up to t = 2300 s during α″$_{iso}$ precipitation, and (3)

a noticeable increase related to α phase precipitation. The slight increase in hardness at t = 150 s is most probably resulting from ω_{iso} precipitation. This subtle change in hardness might be related to a small volume fraction of the aforementioned phase, negligible if compared to the one observed by Williams et al. [38], where the volume fraction of 25% of ω_{iso} influences considerably the mechanical properties of titanium alloys. For that reason and because no single visible ω peak was detected during the analysis of the X-ray diffraction data, ω was not considered for refinement to avoid misleading results. Nonetheless, the presence of ω phase is considered to explain the mechanisms involved in precipitation and phase transformation observed henceforth.

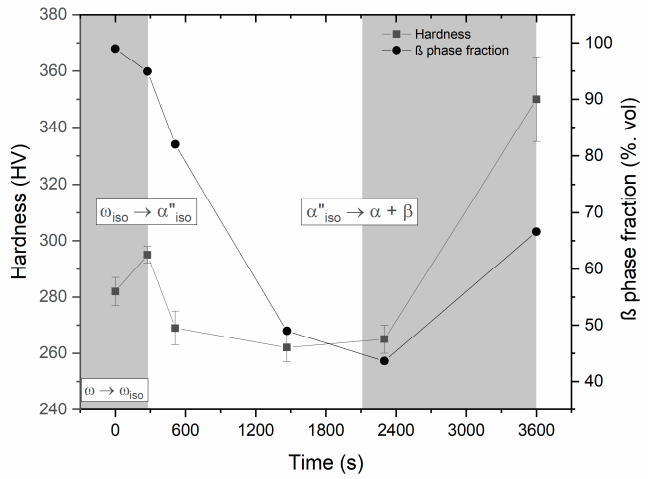

Figure 6. Hardness and β phase fraction evolution along the ageing treatment.

4. Discussion

4.1. Quantitative Analysis of Phase Transformation during Isothermal Treatment

The Rietveld refinement of diffraction patterns was carried out to quantify the present phases during the isothermal treatment. Phase identification was as follows:

1. From t = 0 s β was considered;
2. From t = 300 s α and α''_{iso} volume fraction were considered together. The deconvolution of both phases during refinement was not possible due to presented difficulties; thus, it is not possible to assure that the fraction provided by the refinement for each one of these phases individually is correct, so the summed values were used. The α''_{iso} lattice parameter was taken into account from t = 300 s;
3. From t = 2080 s, the α phase lattice parameter evolution started to be evaluated following the increment of the intensity of {101}α reflections from {111}α″ and {021}α″.

Figure 7 illustrates the refinement as a function of the time for the volume fraction of phases (Figure 7a), the lattice parameter (Figure 7b), and the unit cell volume (Figure 7c). In all three plots, the time (1) refers to the β decomposition onset and the onset of α + α''_{iso} precipitation initiation, time (2) corresponds to the start of α''_{iso} decomposition, and time (3) to the end of the heat treatment. Between t = 300 s and t = 2000 s, the fraction of α + α''_{iso} reaches its maximum value, 59.9%, and then the decomposition of α''_{iso} into α and β begins, raising the volume fraction of β from 40.1% to 66.6% until the end of treatment.

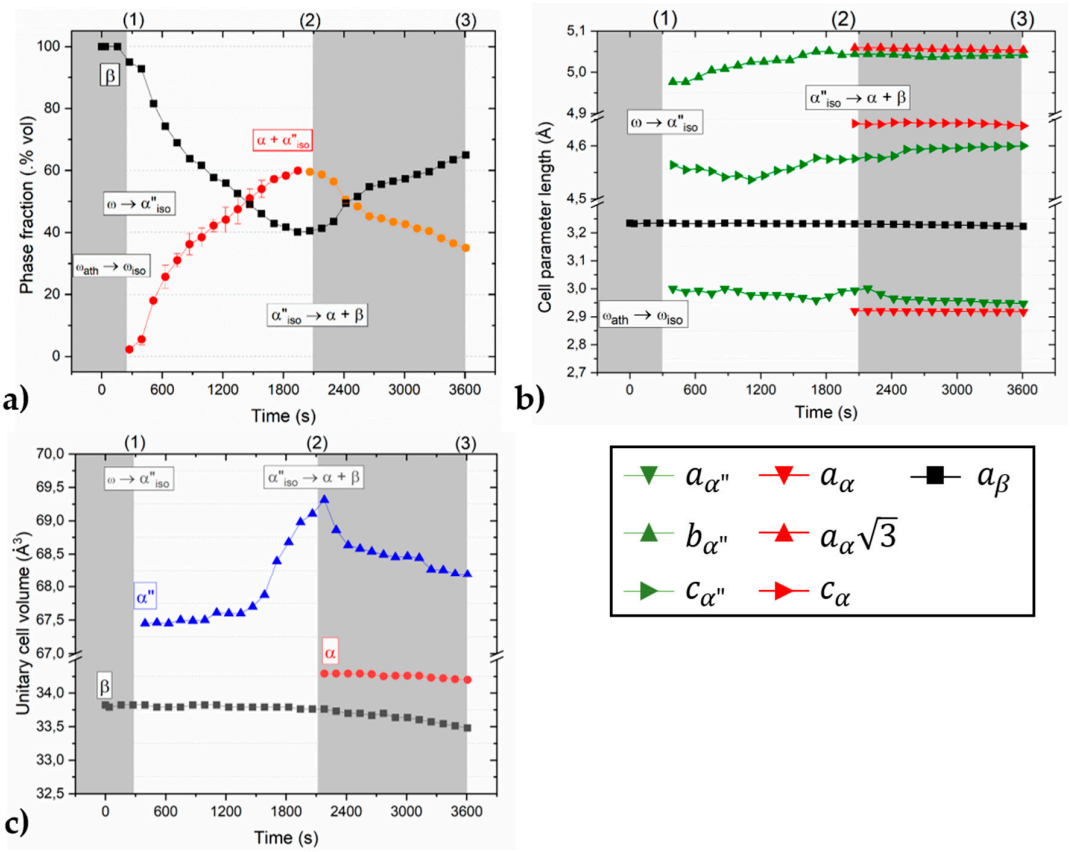

Figure 7. Evolution of (**a**) volume fractions, (**b**) lattice parameters, and (**c**) unit cell volume of phases during ageing at 500 °C for 3600 s of Ti-55531 alloy.

4.2. Behavior of β during Ageing

The volume fraction of β phase decreases continuously during the first 1950 s, reaching a minimum volume of 40.1%. Full width at half maximum (FWHM) values of $\{110\}_{\beta}$ and $\{200\}_{\beta}$ reflections were calculated and depicted in Figure 8, together with the variation of β phase lattice parameter, δa_{β}. The increase of the FWHMs for $\{200\}_{\beta}$ and $\{110\}_{\beta}$ during the heat treatment can be attributed to the precipitation and growth of α and α″$_{iso}$ particles, since it leads to the introduction of microstrains and distortion of the β lattice, and FWHM is rather sensitive to such features [6,10,38].

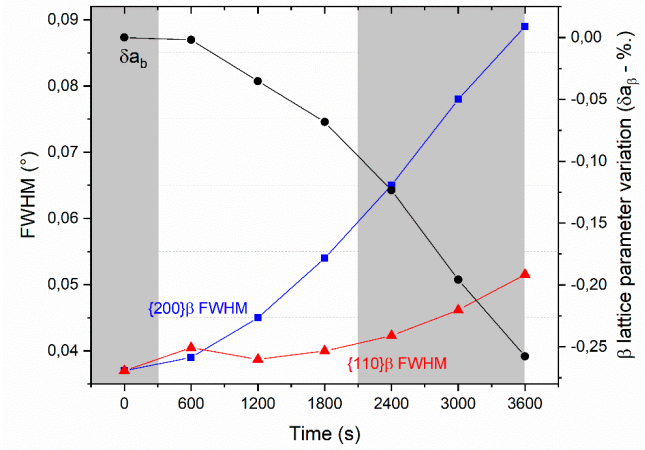

Figure 8. Influence of ageing time on the FWHM of $\{110\}_{\beta}$ and $\{200\}_{\beta}$ peaks and on the variation of a_{β} (δa_{β}).

The decrease of the β unit cell volume (Figure 7c) is more pronounced from t = 2100 s. It is evident that the variation of the cell volume is a direct consequence of the progressive change in the solute content of BCC β lattice, which leads to compositional differences between the matrix and the adjacent areas where precipitates grow, as reported in [38–41]. In addition to this, the change of FWHM can also indicate lattice distortion due to solid solution, i.e., precipitation and growth not only cause the increase in lattice stress but also contribute to the chemical gradient, both of which reflect directly in FWHM rising [10,38]. In this work, the increase in FWHM may result from α phase precipitation and the beginning of isothermal α''_{iso} decomposition, as seen in Figure 7a,c, respectively. Dissolution of α''_{iso} leads to the incorporation of β stabilizers into the matrix at a higher rate, since these elements are barely aggregated by α [42–45]. Therefore, FWHM variations may be an indicator of how the precipitation is evolving and the role of α and α''_{iso} precipitation in the behavior of β during ageing is discernible.

4.3. Precipitation and Decomposition of α''_{iso}

The precipitation of α + α''_{iso} reaches 59.9% of maximum volume at t = ~1950 s, then decreases and reaches 33.4% at t = 3600 s. In Figure 7c it is noted that between the instants t = 400 s and t = 1470 s α''_{iso} unitary cell volume barely increases from 67.4 to 67.7 Å^3. Nonetheless, between t = 1580 s and t = 2200 s, this scenario changes given the substantial increase of such value, from 67.7 to 69.3 Å^3. This increment in volume (hence in $b_{\alpha''}$ and $c_{\alpha''}$ lattice parameters) is followed by the expansion of $y_{\alpha''}$, or the atomic coordinate y of the crystal structure of α''_{iso} phase parallel to b axis, from 0.180 to 0.185. This positive variation is indicative of solute transfer from the matrix to α''_{iso}, as discussed by Banumathy et al. [46]. It is also important to highlight that the value of $c_{\alpha''}$ lattice parameter at the onset of precipitation, ~4.56 Å (Figure 7b), is close to the a parameter of the ω phase, a_ω, ~4.55 Å (Table **1**); this proximity is an indicator that the formation of α''_{iso} may be directly related to ω decomposition [3,9,37,38]. This, together with the fact that the volume fraction of α + α''_{iso} grows whilst β (with some presence of ω) decomposes (Figure 7a) may indicate that precipitation of α + α''_{iso} occurs due to the homogenization of domains resulting from spinodal decomposition of β. This fact can be confirmed by STEM observation in Figure 9 for a sample aged for 1500 s, where the homogenization of spinodal domains can be observed along with EDS results shown in Table 3. The differences in composition decreases especially for Mo, V, and Al if compared to Table 2.

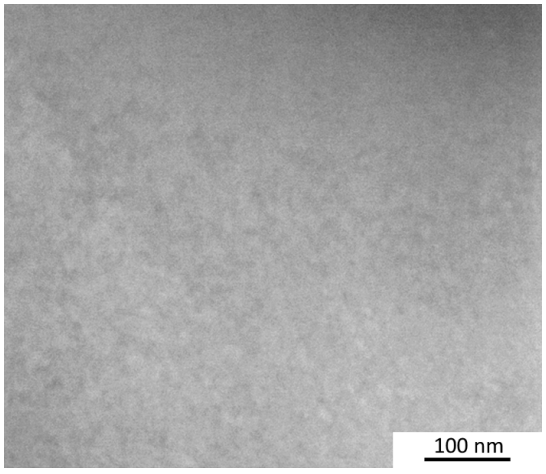

Figure 9. HAADF STEM image of the sample aged at 500 °C for 1500 s, showing homogenization of spinodal domains.

Table 3. Results of EDS analyses for Ti-55531 alloy aged at 500 °C during 1500 s.

Area	Composition (wt %)					
	Ti	Al	Mo	V	Cr	Zr
Dark	81.4	5.5	4.8	4.8	2.6	0.9
Bright	80.2	5.7	4.8	5.1	3.1	1.2

Based on observations of Barriobero-Vila et al. [3] during heating, it can be proposed that the preferential sites for nucleation and growth of α''_{iso} phase are along dislocations, low angle grain boundaries, and the interface of β/β′ spinodal decomposition, where isothermal ω precipitates are located (β/ω interface). Furthermore, the crystal lattice provides favorable pathways to accelerated atomic diffusion (such as distortions). The introduction of solute elements leads to the elimination of stress caused in the lattice by distortions resulting from the dislocations found at β/β′ interfaces. Therefore, precipitation of isothermal α″ in this place leads to the stabilization of β due to the coarsening of β/β′ domains by decreasing the compositional differences in β and β′. Consequently, a decrease in the compositional modulation amplitude takes place.

It is plausible to propose that along with the combined precipitation of α and α''_{iso} phases up to the point at which the $\{101\}_{\alpha}$ reflection stands out from $\{111\}_{\alpha''}$ and $\{021\}_{\alpha''}$ (Figure 5), the value of α''_{iso} volume fraction is higher than α. The precipitation rate of α''_{iso} may be promoted by the spinodal decomposition, favored by the earlier precipitation via $\omega \rightarrow \alpha''_{iso}$ transformation at the β/ω interface [47]. On the other hand, the value of the y-coordinate $y_{\alpha''}$ increases to approach the ideal value to form the BCC structure (y = 0.25), as was also observed for Ti-10V-2Fe-3Al [9]. This means that a possible $\alpha''_{iso} \rightarrow \beta$ transformation also occurs and α''_{iso} has a significant role in the homogenization of spinodal decomposition domains, and thus in the precipitation of α. Therefore, α''_{iso} can be attributed as a "moderator" of transformation kinetics since it is fundamental to the homogenization of spinodal decomposition domains and to the precipitation of α.

4.4. Precipitation and Morphology of α

Regarding the evolution of α lattice parameters, Figure 7b, it is possible to observe a tendency for convergence of α''_{iso} parameters to those of α. Until the end of treatment, $b_{\alpha''}$ and $a_{\alpha}\sqrt{3}$ completely coincide and the $a_{\alpha}/a_{\alpha''}$ pair indicates the same tendency if a longer treatment time is employed. This evolution indicates the gradual transformation of the metastable α''_{iso} phase into the stable α phase assisted by diffusive activity, as reported in literature for Ti-17 and Ti-5553 [5], Ti-10-2-3 [9], and TC21 [48] alloys. With respect to the cell volume of α, Figure 7c, at t = 2100 s when α''_{iso} begins to decompose, both phases have great structural similarity, since $b_{\alpha''}$ and $a_{\alpha}\sqrt{3}$ are already close to each other. This leads one to believe that α is in or very close to chemical equilibrium. Hence, depletion of solute from α''_{iso} is aggregated mainly by β phase, since the decrease of β cell volume is more accentuated than that of α.

SEM images shown in Figure 10 illustrate some characteristic morphologies of α at instants t = 1500, 2300 and 3600 s in β grains. In Figure 10a, the β grains are barely occupied by the intragranular α precipitates, and most of the α is located at the grain boundaries. β grain boundaries are preferred and dominant sites for α nucleation, and despite already precipitating in the early stages of ageing, its volume fraction is still relatively low if compared to the volume of β. When α grows within the β matrix, the strain inherent to this misfit increases and accumulates in the volume of the material. Thus, when stress reaches a critical value, α plates can nucleate and grow intragranularly, increasing its volumetric fraction and evolving as seen in Figure 10d [27].

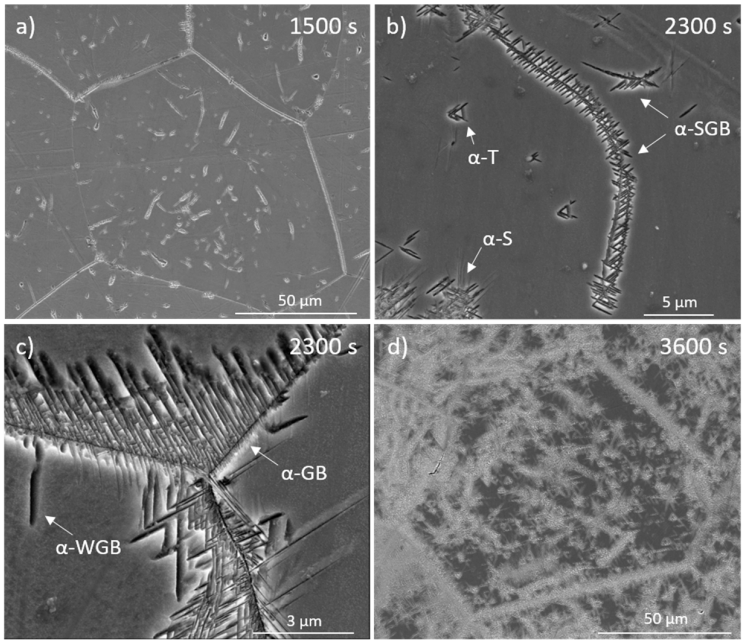

Figure 10. SEM images in SE mode showing (**a**) a β grain at t = 1500 s, (**b**) α phase precipitated from subgrain boundary (α-SGB) and with triangular morphology (α-T) and star-like morphology (α-S), (**c**) a grain boundary with Widmanstätten α (α-WGB), grain boundary α (α-GB), and a mixture of both (α-WGB + α-GB) or the side plates [1] at t = 2300 s, and (**d**) a β grain at t = 3600 s (adapted from [49]).

Figure 10b shows an example of precipitation of α along β subgrain boundaries (α-SGB), isolated triangular (α-T) and star-shaped precipitates (α-S) within the grain. α-T was found by Dehghan-Manshadi and Dippenaar [27] in Ti-5553 alloy aged at 400 °C. According to Balachandran et al. [50], they correspond to the tendency of variant selection of α with respect to β at the moment of precipitation, where α has 3 common <110 >α directions parallel to <111>β arranged in 60° from each other, leading, therefore, to the triangular arrangement. The α stars correspond to the grouping of very thin individual lamellar α-Widmanstätten plates which nucleated and grew from a single nucleus, probably a ω precipitate [27]. On the other hand, Aaronson et al. [51] propose the formation of these plates by the "edge-face" model of sympathetic nucleation, where larger plates form first, followed by the nucleation and growth of the smaller plates from the faces of each other. TEM observations would be necessary to verify which of these models is appropriate for the present case. Recent publications have reported similar microstructural features for Ti-7333 [52] and Ti-5553 [53] under aging conditions.

Figure 10c shows the grain boundary consisting of α-GB, an α-WGB plate, and the set α-WGB + α-GB. The triple-grain boundary is a favorable site to the heterogeneous nucleation of α, since the activation energy in this case is low if compared to other mechanisms found in the matrix. Thus, α finds the ideal site to precipitate and form α-GB, whose morphology consists of a nearly continuous film of this phase. The α-WGB + α-GB colonies are formed from the interface (α-GB/β), consisting of α-WGB plates arranged side by side separated by the remaining β plates, enriched with β-stabilizing elements. Each colony needs a grain containing αGB to form, so they never form directly from the β/β' interface [54].

4.5. Hardness

In Figure 6, as stated before in Section 3.2.2, three main stages of the hardness during the isothermal treatment can be observed. In (1), a slight increment in hardness due to the precipitation of ω_{iso}. In (2) the α''_{iso} precipitation is related to the shearing elastic constant parallel to (110) planes in α''_{iso}, lower than in β phase; for this reason, α''_{iso} is more prone to indentation than β [1]. Hence, as α" precipitation advances, the softening of the material is observed. In (3), the hardness increases by ~35%

from t = 2300 to 3600 s, which is directly related to the acceleration of α precipitation. It is the expected behavior, since α phase plays a fundamental role as a reinforcing element in consequence of its HCP crystal structure. The value obtained after 3600 s of ageing at 500 °C, 350 ± 30 HV, is comparable to the one measured by Jones et al. [4] for Ti-5553 alloy (~380 HV) after 1800 s of ageing at 570 °C, and is related mainly to the morphology and distribution of the fine alpha within the beta grains.

5. Conclusions

Microstructural evolution of Ti-55531 alloy during the early stages of ageing treatment at 500 °C was analyzed by means of in situ high-energy X-ray diffraction. The following conclusions can be drawn regarding this analysis:

- The use of fast heating suppresses any change in the microstructure, restricting the phase transformations to the ageing period.
- During the ageing treatment, the phase transformation follows the sequence $\beta + \omega \rightarrow \beta + \omega_{iso} + \omega \rightarrow \alpha + \alpha''_{iso} + \beta$. The presence of the diffuse streaks is indicative of a transient state.
- The presence of ω phase is confirmed by hardness measurements. The ω phase reflections are not observed in this work and this might be related to the low volume fraction and the superposition of broader and intense β peaks over the ω peaks.
- The isothermal α″ (α″iso) phase may precipitate from the ω phase and mainly from the domains of spinodal decomposition of the β phase, given its role in the homogenization of these domains. This phase is considered to regulate the transformation throughout the studied ageing.
- Based on the evolution of the {111}α″/{021}α″reflection to {101}α, the α phase may nucleate from α″iso, ω phase and β phases. SEM analysis allows the observation of some characteristic morphologies of sympathetic nucleation (α-S) and groups with a tendency to choose preferred directions (α-T), in addition to the preferential precipitation of α along grain boundaries (α-GB), and the Widmanstätten α (α-WGB) formed near to α-GB.

Author Contributions: Conceptualization, R.P.M.G., F.W. and H.C.P.; methodology, R.P.M.G., F.W., B.C., K.A., F.S, F.M. and H.C.P.; validation, R.P.M.G. and B.C.; formal analysis, R.P.M.G. and B.C.; investigation, R.P.M.G., F.W., B.C. and H.C.P.; writing—original draft preparation, R.P.M.G., F.W., B.C., K.A. and H.C.P.; writing—review and editing, R.P.M.G., F.W., B.C., K.A., F.S., F.M. and H.C.P.; supervision, H.C.P. project administration, H.C.P. All authors have read and agreed to the published version of the manuscript.

Funding: This work was supported by the National Council for Scientific and Technological Development (CNPq) with the grants 407399/2013-5, 130674/2015-0 and 161959/2015-6 and by the Coordination for the Improvement of Higher Education Personnel (CAPES) under the project PROBRAL 88881.143948/2017-01.

Acknowledgments: The European Synchrotron Radiation Facility (ESRF) is acknowledged for the provision of synchrotron radiation facilities in the framework of the MA1268 proposal. R.P.M.G. and F.W. would like to thank T. Buslap, P. Barriobero-Vila, G. Requena and D. Canelo-Yubero for the help on the synchrotron experiments and guidance for processing the Data. R.P.M.G. is financially supported by the Austrian Aeronautics Program "TAKE OFF" and the BMVIT-Austrian Ministry for Transport, Innovation, and Technology. In addition, B. C. N. M. de Castilho and N. Colmenares are acknowledged for helping with hardness measurements and discussions, and W. R. Correr is acknowledged for his support and guidance during the heat treatments and microstructural characterization. J.J.C. Pereira is acknowledged for his support on the language corrections.

Conflicts of Interest: The authors declare no conflict of interest.

References

1. Lütjering, G.; Williams, J.C. *Titanium*, 2nd ed.; Springer-Verlag Berlin and Heidelberg GmbH & Co. K: Berlin, Germany, 2007.
2. Moiseyev, V.N. *Titanium Alloys: Russian Aircraft and Aerospace Applications*; CRC Press: Boca Raton, FL, USA, 2006.
3. Barriobero-Vila, P.; Requena, G.; Schwarz, S.; Warchomicka, F.; Buslaps, T. Influence of phase transformation kinetics on the formation of α in a β-quenched Ti–5Al–5Mo–5V–3Cr–1Zr alloy. *Acta Mater.* **2015**, *95*, 90–101. [CrossRef]

4. Jones, N.G.; Dashwood, R.J.; Jackson, M.; Dye, D. β Phase decomposition in Ti-5Al-5Mo-5V-3Cr. *Acta Mater.* **2009**, *57*, 3830–3839. [CrossRef]
5. Aeby-Gautier, E.; Settefrati, A.; Bruneseaux, F.; Appolaire, B.; Denand, B.; Dehmas, M.; Geandier, G.; Boulet, P. Isothermal α" formation in β metastable titanium alloys. *J. Alloys Compd.* **2013**, *577*, S439–S443. [CrossRef]
6. Ivasishin, O.; Markovsky, P.; Semiatin, S.; Ward, C. Aging response of coarse- and fine-grained β titanium alloys. *Mater. Sci. Eng. A* **2005**, *405*, 296–305. [CrossRef]
7. Ivasishin, O.M.; Markovsky, P.E.; Matviychuk, Y.V.; Semiatin, S.L. Precipitation and recrystallization behavior of beta titanium alloys during continuous heat treatment. *Met. Mater. Trans. A* **2003**, *34*, 147–158. [CrossRef]
8. Settefrati, A.; Aeby-Gautier, E.; Dehmas, M.; Geandier, G.; Appolaire, B.; Audion, S.; Delfosse, J. Precipitation in a near Beta Titanium Alloy on Ageing: Influence of Heating Rate and Chemical Composition of the Beta-Metastable Phase. *Solid State Phenom.* **2011**, *172*, 760–765. [CrossRef]
9. Barriobero-Vila, P.; Requena, G.; Warchomicka, F.; Stark, A.; Schell, N.; Buslaps, T. Phase transformation kinetics during continuous heating of a β-quenched Ti–10V–2Fe–3Al alloy. *J. Mater. Sci.* **2015**, *50*, 1412–1426. [CrossRef]
10. Aeby-Gautier, E.; Bruneseaux, F.; Teixeira, J.D.C.; Appolaire, B.; Geandier, G.; Denis, S. Microstructural formation in Ti alloys: In-situ characterization of phase transformation kinetics. *JOM* **2007**, *59*, 54–58. [CrossRef]
11. Liss, K.-D.; Bartels, A.; Schreyer, A.; Clemens, H. High-Energy X-Rays: A tool for Advanced Bulk Investigations in Materials Science and Physics. *Textures Microstruct.* **2003**, *35*, 219–252. [CrossRef]
12. Liss, K.-D.; Yan, K. Thermo-mechanical processing in a synchrotron beam. *Mater. Sci. Eng. A* **2010**, *528*, 11–27. [CrossRef]
13. Liss, K.D. Thermo-Mechanical Processing in a Synchrotron Beam—From Simple Metals To Multiphase Alloys and Intermetallics. *World J. Eng.* **2010**, *7*, 438.
14. Warchomicka, F.; Yubero, C.-; Zehetner, E.; Requena, G.; Stark, A.; Canelo-Yubero, D.; Poletti, C. In-Situ Synchrotron X-Ray Diffraction of Ti-6Al-4V During Thermomechanical Treatment in the Beta Field. *Met.* **2019**, *9*, 862. [CrossRef]
15. Liss, K.-D.; Whitfield, R.E.; Xu, W.; Buslaps, T.; Yeoh, L.A.; Wu, X.; Zhang, D.; Xia, K. In situsynchrotron high-energy X-ray diffraction analysis on phase transformations in Ti–Al alloys processed by equal-channel angular pressing. *J. Synchrotron Radiat.* **2009**, *16*, 825–834. [CrossRef] [PubMed]
16. Bania, P.J. Beta titanium alloys and their role in the titanium industry. *JOM* **1994**, *46*, 16–19. [CrossRef]
17. Nag, S.; Zheng, Y.; Williams, R.; Devaraj, A.; Boyne, A.; Wang, Y.; Collins, P.; Viswanathan, G.; Tiley, J.; Muddle, B.; et al. Non-classical homogeneous precipitation mediated by compositional fluctuations in titanium alloys. *Acta Mater.* **2012**, *60*, 6247–6256. [CrossRef]
18. The FIT2D Home Page. Available online: http://www.esrf.eu/computing/scientific/FIT2D/ (accessed on 20 October 2019).
19. ImageJ. Available online: https://imagej.nih.gov/ij/ (accessed on 20 October 2019).
20. MAUD—Material Analys Using Diffraction. Available online: http://maud.radiographema.eu/ (accessed on 20 October 2019).
21. Banerjee, S.; Mukhopadhyay, P. *Phase Transformations: Examples from Titanium and Zirconium Alloys*; Elsevier: Amsterdam, The Netherlands, 2007; Volume 1.
22. Basak, C.B.; Neogy, S.; Srivastava, D.; Dey, G.; Banerjee, S. Disordered bcc γ-phase to δ-phase transformation in Zr-rich U-Zr alloy. *Philos. Mag.* **2011**, *91*, 3290–3306. [CrossRef]
23. Obbard, E.G.; Hao, Y.L.; Talling, R.J.; Li, S.J.; Zhang, Y.W.; Dye, D.; Yang, R. The effect of oxygen on α" martensite and superelasticity in Ti-24Nb-4Zr-8Sn. *Acta Mater.* **2011**, *59*, 112–125. [CrossRef]
24. Li, T.; Kent, D.; Sha, G.; Stephenson, L.T.; Ceguerra, A.V.; Ringer, S.P.; Dargusch, M.S.; Cairney, J.M. New insights into the phase transformations to isothermal ω and ω-assisted α in near β-Ti alloys. *Acta Mater.* **2016**, *106*, 353–366. [CrossRef]
25. Liss, K.-D.; Stark, A.; Bartels, A.; Clemens, H.; Buslaps, T.; Phelan, D.; Yeoh, L.A. Directional Atomic Rearrangements During Transformations Between the α- and γ-Phases in Titanium Aluminides. *Adv. Eng. Mater.* **2008**, *10*, 389–392. [CrossRef]
26. Settefrati, A.; Dehmas, M.; Geandier, G.; Denand, B.; Aeby-Gautier, E.; Appolaire, B.; Khelifati, G.; Delfosse, J. *Precipitation sequences in beta metastable phase of Ti-5553 alloy during ageing. Ti-2011*; Science Press Beijing: Beijing, China, 2011; pp. 468–472.

27. Dehghan-Manshadi, A.; Dippenaar, R.J. Development of α-phase morphologies during low temperature isothermal heat treatment of a Ti–5Al–5Mo–5V–3Cr alloy. *Mater. Sci. Eng. A* **2011**, *528*, 1833–1839. [CrossRef]
28. Porter, D.A.; Easterling, K.E.; Sherif, M. *Phase Transformations in Metals and Alloys*; CRC Press: Boca Raton, FL, USA, 2009.
29. Zheng, Y.; Sosa, J.M.; Fraser, H.L. On the Influence of Athermal ω and α Phase Instabilities on the Scale of Precipitation of the α Phase in Metastable β-Ti Alloys. *JOM* **2016**, *68*, 1343–1349. [CrossRef]
30. Contrepois, Q.; Carton, M.; Lecomte-Beckers, J. Characterization of the β Phase Decomposition in Ti-5Al-5Mo-5V-3Cr at Slow Heating Rates. *Open J. Met.* **2011**, *1*, 1–11. [CrossRef]
31. Ramsteiner, I.; Shchyglo, O.; Mezger, M.; Udyansky, A.; Bugaev, V.; Schöder, S.; Reichert, H.; Dosch, H. Omega-like diffuse X-ray scattering in Ti–V caused by static lattice distortions. *Acta Mater.* **2008**, *56*, 1298–1305. [CrossRef]
32. Banerjee, S.; Tewari, R.; Dey, G.K. Omega phase transformation-morphologies and mechanisms. *Int. J. Mater. Res.* **2006**, *97*, 963–977. [CrossRef]
33. Mittemeijer, E.J.; Scardi, P. *Diffraction Analysis of the Microstructure of Materials*; Springer: New York, NY, USA, 2013.
34. Settefrati, A.; Aeby-Gautier, E.; Appolaire, B.; Dehmas, M.; Geandier, G.; Khelifati, G. Low temperature transformation in the β-metastable Ti 5553 alloy. *Mater. Sci. Forum* **2013**, *738–739*, 97–102. [CrossRef]
35. Sabeena, M.; Murugesan, S.; Mythili, R.; Sinha, A.K.; Singh, M.N.; Vijayalakshmi, M.; Deb, S.K. Studies on ω Phase Formation in Ti-Mo Alloys Using Synchrotron XRD. *Trans. Indian Inst. Met.* **2014**, *68*, 1–6. [CrossRef]
36. Šmilauerová, J.; Harcuba, P.; Kriegner, D.; Janecek, M.; Holý, V. Growth kinetics of ω particles in β-Ti matrix studied by in-situ small-angle x-ray scattering. *Acta Mater.* **2015**, *100*, 126–134. [CrossRef]
37. Nejezchlebová, J.; Janovská, M.; Seiner, H.; Sedlák, P.; Landa, M.; Šmilauerová, J.; Stráský, J.; Harcuba, P.; Janeček, M. The effect of athermal and isothermal ω phase particles on elasticity of β-Ti single crystals. *Acta Mater.* **2016**, *110*, 185–191. [CrossRef]
38. Williams, J.C.; Hickman, B.S.; Marcus, H.L. The effect of omega phase on the mechanical properties of titanium alloys. *Metall. Trans.* **1971**, *2*, 1913–1919. [CrossRef]
39. Laughlin, D.E.; Cahn, J.W. Spinodal decomposition in age hardening copper-titanium alloys. *Acta Met.* **1975**, *23*, 329–339. [CrossRef]
40. Geandier, G.; Aeby-Gautier, E.; Settefrati, A.; Dehmas, M.; Appolaire, B. Study of diffusive transformations by high energy X-ray diffraction. *Comptes Rendus Phys.* **2012**, *13*, 257–267. [CrossRef]
41. Barriobero-Vila, P.; Requena, G.; Buslaps, T.; Alfeld, M.; Boesenberg, U. Role of element partitioning on the α–β phase transformation kinetics of a bi-modal Ti–6Al–6V–2Sn alloy during continuous heating. *J. Alloy. Compd.* **2015**, *626*, 330–339. [CrossRef]
42. Chen, F.; Xu, G.; Zhou, K.; Zhang, X. Exploring the Phase Transformation in β-Quenched Ti-55531 Alloy During Continuous Heating via Dilatometric Measurement, Microstructure Characterization, and Diffusion Analysis. *Met. Mater. Trans. A* **2016**, *47*, 5383–5394. [CrossRef]
43. Elmer, J.; Palmer, T.; Babu, S.; Specht, E. In situ observations of lattice expansion and transformation rates of α and β phases in Ti–6Al–4V. *Mater. Sci. Eng. A* **2005**, *391*, 104–113. [CrossRef]
44. Mantani, Y.; Tajima, M. Phase transformation of quenched α″ martensite by aging in Ti-Nb alloys. *Mater. Sci. Eng. A* **2006**, *438–440*, 315–319. [CrossRef]
45. Mantani, Y.; Takemoto, Y.; Hida, M.; Sakakibara, A.; Tajima, M. Phase Transformation of α″ Martensite Structure by Aging in Ti-8 mass%Mo Alloy. *Mater. Trans.* **2004**, *45*, 1629–1634. [CrossRef]
46. Banumathy, S.; Mandal, R.K.; Singh, A.K. Structure of orthorhombic martensitic phase in binary Ti–Nb alloys. *J. Appl. Phys.* **2009**, *106*, 093518. [CrossRef]
47. Ohmori, Y.; Ogo, T.; Nakai, K.; Kobayashi, S. Effects of ω-phase precipitation on β → α, α″ transformations in a metastable β titanium alloy. *Mater. Sci. Eng. A* **2001**, *312*, 182–188. [CrossRef]
48. Tang, B.; Kou, H.C.; Wang, Y.H.; Zhu, Z.S.; Zhang, F.S.; Li, J.S. Kinetics of orthorhombic martensite decomposition in TC21 alloy under isothermal conditions. *J. Mater. Sci.* **2012**, *47*, 521–529. [CrossRef]
49. Guimarães, R.P.M. Estudo in situ da solubilização e do envelhecimento da liga β-metaestável Ti-5Al-5Mo-5V-3Cr-1Zr usando difração de raio-X com luz síncrotron de alta energia. Master's Dissertation, Escola de Engenharia de São Carlos, University of São Paulo, São Carlos, Brazil, 2018. [CrossRef]

50. Balachandran, S.; Kashiwar, A.; Choudhury, A.; Banerjee, D.; Shi, R.; Wang, Y. On variant distribution and coarsening behavior of the α phase in a metastable β titanium alloy. *Acta Mater.* **2016**, *106*, 374–387. [CrossRef]
51. Aaronson, H.; Spanos, G.; Masamura, R.; Vardiman, R.; Moon, D.; Menon, E.; Hall, M. Sympathetic nucleation: An overview. *Mater. Sci. Eng. B* **1995**, *32*, 107–123. [CrossRef]
52. Dong, R.; Li, J.; Kou, H.; Fan, J.; Tang, B.; Sun, M. Precipitation behavior of α phase during aging treatment in a β-quenched Ti-7333. *Mater. Charact.* **2018**, *140*, 275–280. [CrossRef]
53. Manda, P.; Singh, V.; Chakkingal, U.; Singh, A. Development of α precipitates in metastable Ti-5Al-5Mo-5V-3Cr and similar alloys. *Mater. Charact.* **2016**, *120*, 220–228. [CrossRef]
54. Salib, M.; Teixeira, J.; Germain, L.; Lamielle, E.; Gey, N.; Aeby-Gautier, E. Influence of transformation temperature on microtexture formation associated with α precipitation at β grain boundaries in a β metastable titanium alloy. *Acta Mater.* **2013**, *61*, 3758–3768. [CrossRef]